NUMERICAL SIMULATION OF WATER ENTRY WITH FLOW DETACHMENT

C. M. Bao[1], G. X. Wu*[1, 2], G. D. Xu[1]

1. College of Shipbuilding Engineering, Harbin Engineering University, Harbin 150001, P. R. China;

2. Department of Mechanical Engineering, University College London, London WC1E 7JE, UK;

Abstract

A two-dimensional finite wedge entering water obliquely at a prescribed speed is considered through the velocity potential theory for the incompressible liquid. The gravity is also included. The problem is solved by using the boundary element method in the time domain. The method of the stretched coordinate system is adopted at the initial stage. A condition is imposed at the intersection of the free surface and the body surface after flow detachment to allow the liquid to leave the body surface smoothly. A new methodology is developed to treat free jet with free surface on both sides. The auxiliary function method is used to calculate the pressure on the body surface. Detailed results for the free surface shape and pressure distribution are provided, and the effect of physical parameters on water entry are discussed.

Keywords: Water entry; Fully nonlinear boundary conditions; Boundary element method; Stretched coordinate system; Flow detachment; Free jet flow.

1. Introduction

Fluid/structure impact though a solid body entering the surface of a liquid is a common problem in naval architecture, ocean engineering, coastal engineering and many other areas. In the mathematical modelling and numerical simulation, a solid two dimensional wedge is a typical example. Based on the assumption of inviscid and incompressible liquid, Dobrovol'skaya (1969) obtained a self-similar solution for a wedge in vertical entry with constant speed, using the conformal mapping in which the complex velocity potential satisfied the nonlinear free surface boundary condition. Zhao & Faltinsen (1993) considered the same problem using the boundary element method in the time domain. The thin jet was cut near its tip. Wu *et al*. (2004) solved the problem through using the Cauchy theorem for the complex potential and the jet was approximated using the shallow equation. This was extended by Xu *et al*. (2008) for the problem of oblique entry of an asymmetric wedge. Adopting the integral hodograph method and using the velocity magnitude and direction as the variables, Semenov & Iafrati (2006) solved the problem of vertical water entry of an asymmetric wedge.

The above work is principally for a wedge of infinite length, in which the flow will never depart from the wedge. In reality, a wedge has finite height. The flow will depart from the body when it has passed the knuckle. In such a case, the flow characters and solution procedure will be verymuch different. One noticeable example is that the flow for the wedge will no longer be self-similar even

*Corresponding author. Tel.: +44 20 7679 3870; fax: +44 20 7388 0180.

E-mail address: g.wu@ucl.ac.uk (G.X. Wu)

at constant speed and zero gravity. Relative to the non-separated flow, there has been far less work on water entry with flow detachment from the body surface. Zhao *et al.* (1996) considered the problem of water entry beyond the stage that the flow has passed the knuckle of the wedge. The velocity continuity condition was imposed at the separation point. Gravity effect was ignored and the jet was cut. Experimental study was undertaken at the same time. This model was been extended for planning vessels by Sun *et al.* (2007). Tassin *et al.* (2014) used an analytical model based on the Logvinovich model for water entry of a finite wedge with flow separation. While the above work is based on the potential flow, Oger *et al.* (2006) used the smooth particles hydrodynamics (SPH) method to simulate water entry of an asymmetric wedge while Gu *et al.* (2014) used the level setting method. In experiment, the photos in Greenhow & Lin (1983) and Judge *et al.* (2004) also show some very interesting features of the flow after the free surface has detached from the body.

The present paper considers the water entry of a finite wedge in a prescribed speed. The gravity is also included, which was shown by Sun *et al.* (2015) becoming more important as time increases. When flow departs from the body, it is assumed that the particle will leave the body tangentially. Thus the slopes of the free surface and the body surface will be the same at the separation point. The normal velocity will then be continuous at the point. Before flow separation, the jet attached on the free surface will be treated using the shallow water equation (Wu, 2007). After flow separation, both sides of the jet become the free surface. It is found that such a treatment is not always numerically satisfactory. Instead, a new method is proposed based on the fact that the jet in such a case will be virtually in free fall motion. Detailed results for the free surface shape and pressure distribution are given and their physics is discussed.

2. Mathematical model and numerical procedure

2.1 Governing equation and boundary conditions

A two-dimensional finite wedge entering water obliquely at a prescribed speed is considered here, which has left deadrise angle γ_1 and right deadrise angle γ_2 as shown in Fig. 1. We define a Cartesian coordinate system $O-xy$ fixed in the space, in which *x*-axis is along the undisturbed water surface and *y*-axis is vertically upwards. At $t=0$, the tip of the wedge is at the origin of the system. The translational velocity of the wedge is $\boldsymbol{U}=U\boldsymbol{i}-V\boldsymbol{j}$, where $\boldsymbol{i}$ and $\boldsymbol{j}$ are the unit vectors in the x and y directions respectively. Here the minus sign before V means that it is positive when the body moves downwards. The wedge has finite height with breadth B at the top and its half inner angle, or the angle between its symmetry line (dashed line in the figure) and its face is γ. Heel angle θ is the angle between the symmetry line and the y axis. These angles form the following relationships:

$$\gamma_1=\frac{\pi}{2}+\theta-\gamma,\gamma_2=\frac{\pi}{2}-\theta-\gamma \tag{1}$$

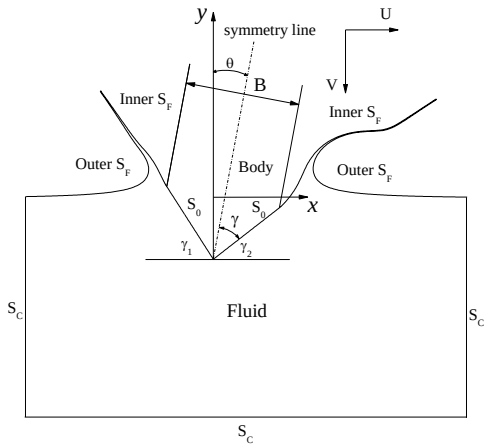

Fig. 1 *Sketch of the problem*

The fluid is assumed to be incompressible and inviscid, and the flow irrotational. A velocity potential ϕ can then be introduced, which satisfies Laplace equation

$$\nabla^2\phi = 0 \tag{2}$$

in the fluid domain. On the body surface S_0, we have from the impermeable condition

$$\frac{\partial\phi}{\partial n} = \boldsymbol{U}\bullet\boldsymbol{n} = U\bullet n_x - V\bullet n_y \tag{3}$$

where $\boldsymbol{n} = (n_x, n_y)$ is the normal vector of the body surface pointing out of the fluid domain. The Lagrangian form of the kinematic and dynamic conditions on the free surface S_F can be written as

$$\frac{Dx}{Dt} = \frac{\partial\phi}{\partial x}, \frac{Dy}{Dt} = \frac{\partial\phi}{\partial y} \tag{4}$$

$$\frac{D\phi}{Dt} = -gy + \frac{1}{2}\left|\nabla\phi\right|^2 \tag{5}$$

where g is the acceleration due to gravity and the atmospheric pressure has been assumed to be constant in Eq. (5). In addition, we specify a far-field condition

$$\phi \to 0 \tag{6}$$

at $\sqrt{x^2+y^2} \to \infty$ on the basis that the fluid there is undisturbed.

At the initial stage of water entry, only a tiny part of the body moves into the water. In order to maintain sufficient numerical accuracy, extremely small elements in numerical solution would be needed in the physical system $O-xy$. The fluid domain disturbed by the wedge entry increases as the wetted body surface increases. Hence, in a fixed computational domain, a large number of elements would be needed which would become impractical in the numerical calculation. Thus, the method of the stretched coordinate system is adopted (Wu, 2007). We define

$$\phi(x,y,t) = s(t)\varphi(\alpha,\beta,t), \alpha = x/s(t), \beta = y/s(t) \tag{7}$$

where $s(t)$ is the vertical displacement of the wedge:

$$s(t)=\int_0^t V(\tau)d\tau \tag{8}$$

together with the horizontal displacement

$$h(t)=\int_0^t U(\tau)d\tau \tag{9}$$

In the stretched coordinate system, the free surface condition can be written as

$$\frac{D(s\alpha)}{Dt}=\frac{\partial\varphi}{\partial\alpha},\frac{D(s\beta)}{Dt}=\frac{\partial\varphi}{\partial\beta} \tag{10}$$

$$\frac{D(s\varphi)}{Dt}=-gs\beta+\frac{1}{2}\left(\varphi_\alpha^2+\varphi_\beta^2\right) \tag{11}$$

When the flow separates at the knuckle, the computation may be done in the physical domain directly.

2.2 Numerical procedure

To solve the above boundary value problem, we convert the differential equation in the fluid domain into the following boundary integral equation based on Green's second identity,

$$A(p)\varphi(p)=\int_S\left[\ln r_{pq}\frac{\partial\varphi(q)}{\partial n_q}-\varphi(q)\frac{\partial}{\partial n_q}\left(\ln r_{pq}\right)\right]dS_q \tag{12}$$

where $A(\mathrm{p})$ is the solid angle of point p on the body surface, and r_{pq} is the distance between points p and q. The integration is performed over the whole boundary S of the fluid domain, including the free surface S_F, the body surface S_0 as well as the control surface S_C away from the body.

The boundary of the fluid domain is discretized into straight-line elements. On each element, the values of φ and φ_n are defined at the both nodes and their values within the element can be obtained by using shape function. We have

$$f=\sum_{i=1}^{2}N_i(\xi)f_i=N_1(\xi)f_1+N_2(\xi)f_2 \tag{13}$$

where f stands for either φ or φ_n, and

$$N_1(\xi)=1-\xi,N_2(\xi)=\xi \tag{14}$$

The local coordinate ξ in the above equations is the distance along the element varying from 0 at one node to 1 at the other. Eq. (12) can then be written as

$$A(p)\varphi(p)+\sum_{k=1}^{N_e}\sum_{i=1}^{2}\varphi_k^i(q)\int_0^1\frac{\partial}{\partial n_q}\left(\ln r_{pq}\right)N_i(\xi)l_k d\xi=\sum_{k=1}^{N_e}\sum_{i=1}^{2}\frac{\partial\varphi_k^i(q)}{\partial n_q}\int_0^1\ln r_{pq}N_i(\xi)l_k d\xi \tag{15}$$

where $i=1,2$ respectively denote the first and second nodes of the k th element with length l_k

and N_e is the total number of elements. We let point p approach each element node on the boundary. This leads to the following matrix equation:

$$[H]\{\varphi\} = [G]\{\varphi_n\} \tag{16}$$

where the matrices $[H]$ and $[G]$ contain the integrals of $\frac{\partial}{\partial n_q}\left(\ln r_{pq}\right)$ and $\ln r_{pq}$ over each element, respectively, and $\{\varphi\}$ and $\{\varphi_n\}$ are columns containing the potentials and its normal derivatives on all the element nodes.

The normal derivative of the potential on the body surface and the potential on the free surface are known at each time step. They are moved to the right hand side of the equation, while the unknowns are moved to the left. Eq. (15) can then be rearranged as (Lu *et al.*, 2000)

$$\left[H^{S_0} \; -G^{S_F} \; H^{S_C}\right]\begin{Bmatrix}\varphi^{S_0}\\ \varphi_n^{S_F}\\ \varphi^{S_C}\end{Bmatrix} = \left[G^{S_0} \; -H^{S_F} \; G^{S_C}\right]\begin{Bmatrix}\varphi_n^{S_0}\\ \varphi^{S_F}\\ \varphi_n^{S_C}\end{Bmatrix} \tag{17}$$

where the superscripts correspond to the surfaces defined in Fig. 1. Once the solution of Eq. (17) at each time step has been obtained, we can update the free surface profile through the kinematic boundary conditions given by Eq. (4) while the dynamic boundary condition in Eq. (5) is used to update the velocity potential on the free surface.

Before flow separates from the knuckle, the treatments used for the jet developed along the body surface and for the intersection of the body surface and the free surface are similar to those used previously (Wu, 2007). For the former, the shallow water assumption is used. For the latter the velocity potential is continuous at the intersection and is known at each time. φ_n is discontinuous, and it is known when it is viewed from the body surface but unknown from the free surface and the unknown can be obtained from the solution of Eq. (17).

2.3 Treatment of flow detachment and potential at the intersection

When the flow departs from the knuckle, the separation point becomes the intersection of the free surface and the body surface. It is assumed that the flow leaves the knuckle tangentially and the following steps are then taken in the numerical simulation. We note that the fluid particle $A^{(i)}$ at the knuckle at time $t^{(i)}$ will move to $A^{(i+1)}$ at time $t^{(i+1)} = t^{(i)} + dt$. Its location and the potential at $A^{(i+1)}$ can be obtained based on Eqs. (4) and (5), with the assumption that the direction of line $A^{(i)}$ and $A^{(i+1)}$ is the tangential direction of the wedge surface. The knuckle will be occupied by a different fluid particle $B^{(i+1)}$ at time $t^{(i+1)}$. The potential there could be obtained by using

$$\begin{aligned}\frac{D\phi}{Dt} &= \frac{\partial\phi}{\partial t} + \boldsymbol{U}\bullet\nabla\phi \\ &= \boldsymbol{U}\bullet\nabla\phi - \frac{1}{2}\nabla\phi\bullet\nabla\phi - gy\end{aligned} \tag{18}$$

However, we shall use an alternative method. As the flow is assumed to leave the body surface tangentially at the knuckle, we have

$$\left.\frac{\partial \phi}{\partial l}\right|_{-} = \left.\frac{\partial \phi}{\partial l}\right|_{+} \tag{19}$$

where $\left.\frac{\partial \phi}{\partial l}\right|_{-}$ and $\left.\frac{\partial \phi}{\partial l}\right|_{+}$ denote the derivatives in the tangential direction at the knuckle from the free surface or the body surface, respectively. We then have the right number of equations to solve Eq. (17) for the unknowns.

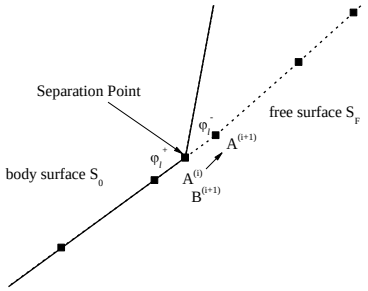

Fig. 2 The node at separation point

2.4 Jet treatment after liquid detachment from the knuckle

A major feature of the present work is that the wedge has finite length. When it enters water, flow along the wedge surface will eventually detach from the knuckle. In most cases, this is in the form of a jet, or a thin layer liquid. When it departs from the wedge, both sides of the jet become the free surface, or a free jet has been formed. Unlike the jet attached to the body surface, the position of a free jet cannot be controlled by the location of the rigid surface in the numerical calculation. Its movement is very prone to the numerical error. On the other hand, the accuracy in the jet region is not easy to control unless elements with size much smaller than jet width are used. This is wholly impractical from computational point of view. Zhao *et al.* (1996) and Sun (2007) cut most of the tip of the jet flow. In the present work, we shall introduce a different treatment for the free jet.

The Euler equations, or the NS equation without viscosity, can be written as:

$$\frac{D\boldsymbol{u}}{Dt} = -\frac{1}{\rho}\nabla p - g\,\boldsymbol{j} \tag{20}$$

where ρ is the density of the fluid, $\boldsymbol{u} = \nabla\phi$ is the fluid velocity. We may apply the equation to a thin free jet. We notice that the pressure p on the both sides of the jet is constant and its tangential derivative is then zero. When the jet is very thin, the derivation across the jet will be also zero. Thus we have $\nabla p = 0$. Eq. (20) becomes

$$\frac{D\boldsymbol{u}}{Dt} = -g\,\boldsymbol{j} \tag{21}$$

This means that the velocity in the jet can be obtained directly without the solution of the potential.

This avoids the numerical difficulty in Eq. (17) when it is used in the thin free jet.

2.5 Impact pressure

When the potential has been found, the Bernoulli equation can be used to obtain the total pressure:

$$P_T = -\rho\left(\phi_t + \frac{1}{2}\nabla\phi\nabla\phi + gy\right) \tag{22}$$

One difficulty is how to deal with the ϕ_t term, which is still not explicitly known even when ϕ is found. It could be obtained by a difference method with respect to time using the potential at the previous time step, but such a procedure is usually not accurate enough. Here we adopt the approach proposed by Wu & Eatock Taylor (2003). We notice that ϕ_t satisfies the Laplace equation. Its free surface boundary condition can be obtained by letting Eq. (22) be equal to zero

$$\phi_t = -\frac{1}{2}\nabla\phi\nabla\phi - gy \tag{23}$$

As we consider only the translational motion here, the body surface boundary condition can be written as (Wu, 1998):

$$\frac{\partial\phi_t}{\partial n} = \dot{\boldsymbol{U}}\bullet\boldsymbol{n} - \boldsymbol{U}\bullet\frac{\partial\nabla\phi}{\partial n} \tag{24}$$

The problem of ϕ_t can then be solved in a manner similar to that used for ϕ and the pressure in Eq. (22) can be obtained.

3. Numerical results and discussions

ρ, g and B are used for the nondimensionalisation. Thus Froude number $F_n = V/(gB)^{1/2}$ and $\tau = s(t)/B$ are used to define the vertical velocity and the vertical distance that the wedge has travelled, $C_P = P_T / 0.5\rho V^2$ is used to show the pressure.

We start the simulation at $\tau = \tau_0$ which can be chosen arbitrarily small. At such a small distance, the overall disturbance to the liquid is small. The initial solution can be chosen for the computational convenience as the result does not have large effect on the flow at later stage. Thus it can be selected to ensure that the simulation can move forward smoothly with the time step. Here we adopt the similarity solution as the initial solution at τ_0, as done by Xu *et al.*(2008), and then use the time stepping method onwards. The computational domain is chosen as a rectangular control box which is truncated at $\alpha = \pm\max(20, 20/\tan\gamma_i)$ and β =-40 in the stretched coordinate system.

Elements of typical length Δl are uniformly distributed on the body surface S_0. Before flow separation, the same elements are used on the free surface near the body. On the free surface away from the body, the size of the element increases gradually at a fixed ratio, and the largest element far away from the body is about five times typical length Δl. After the flow detaches from the

knuckle of the body, a local mesh refinement is used near the tip of the jet and the separation point

The time Δt is chosen to ensure sufficient accuracy which is determined by

$$\Delta t \le C \frac{\min(\Delta l)}{\max(|(\nabla \phi)_{SF}|)} \tag{25}$$

where $0 < C < 1$ is to ensure that the fluid particle on the free surface will move a small fraction of grid size within one time step. When the free surface deforms as time increases, elements can be distorted severely and remeshing is therefore applied regularly based on the scheme in Sun (2007).

3.1 Convergence study and comparison

We first verify our methodology and numerical procedure through convergence study. We consider the case of a wedge of $\gamma = \pi/4$ and $\theta = 0$ entering vertically into water at constant speed of $F_n = 2$.

We set the typical element length $\Delta l = 0.04$, 0.03 and 0.02 respectively in the stretched system. The simulation starts at $\tau_0 = 0.001$. Fig. 3 gives the free surface profile and the pressure distribution after flow separation at $\tau = 0.3$ and $\tau = 0.6$. The results corresponding to different meshes are in a good agreement. This shows that the present method is already mesh independent. To verify convergence with the time step, we choose $C = 0.4$, 0.3 and 0.2 respectively. Fig. 4 gives results at $\tau = 0.3$ and $\tau = 0.6$ and it can be seen that convergence has been achieved. C is taken as 0.3 in the following simulations together with $\Delta l = 0.03$.

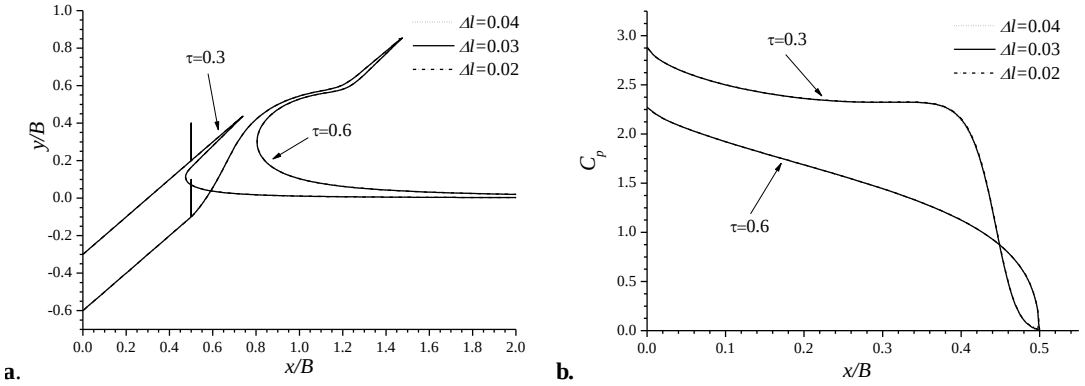

Fig. 3 Mesh convergence study ($\tau = 0.3, \tau = 0.6$), (a) free surface profile, (b) total pressure distribution on the wedge surface

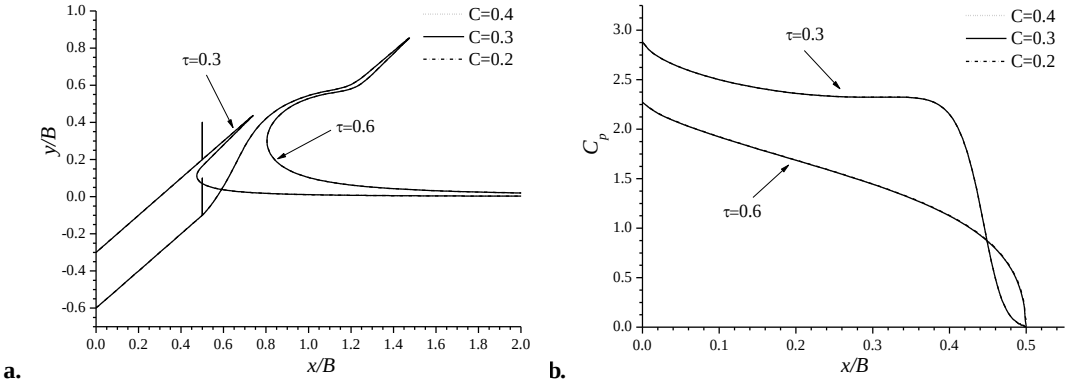

Fig. 4 Time step convergence study ($\tau = 0.3, \tau = 0.6$), (a) free surface profiles, (b) total pressure distribution on the wedge surface

To further validate our simulation, we may make comparison for the cases which have been solved previously by others. Before the fluid detachment from the body surface, the problem is the same as that for an infinite wedge. The comparison for such a case has given a good agreement in our numerical tests. For the problem with detachment, we consider the case of a symmetric wedge with $B = 0.5\,m$ and $\gamma = 60^{\circ}$ entering water vertically with the prescribed velocity given by Zhao *et al.* (1996). In their simulation, the gravity was neglected. The wedge motion follows that experimentally measured motion, as shown in Fig. 5.

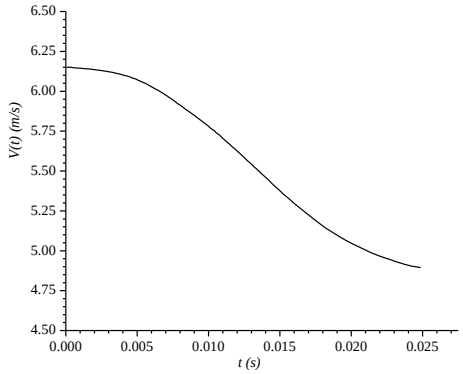

Fig. 5 The velocity history from Zhao *et al.* (1996)

Discrete values of the velocity are obtained from Fig. 5 through software. Four point Lagrangian interpolation formula is used $\boldsymbol{U}$ from which the acceleration $\dot{\boldsymbol{U}}$ in Eq. (24) is obtained from direct differentiation. The pressure distributions at $\tau = 0.0087$, 0.0316 and 0.0404 obtained from the present simulations are given in Fig.6, which are already time step and mesh independent. The results agree fairly well with the experiment data and numerical results of Zhao *et al.* (1996) at $\tau =$ 0.0087 before separation, shown in Fig. 6a. However, discrepancy becomes much more obvious after separation. As mentioned by Zhao *et al.* (1996), the three dimensional effect becomes more significant at this stage in the experiment. This could be part of the reason for lager difference between numerical results and experiment data. At later stages in Figs. 6b and 6c the flow has separated from the body. In the work of Zhao *et al.* (1996), the jet was cut from the simulation at its

relatively earlier stage. When the truncation after jet cutting reaches the knuckle an artificial jet with constant thickness and a hemicircle at its end was introduced and attached on the truncation. In the present time step and mesh independent results, jet has always been part of the solution. This could be part of the reason for the discrepancy between the two set of results. Another possibility could be that Zhao *et al.* (1996) has ignored the effect of the gravity. Simulations are then undertaken by removing g completely from the dynamic free surface boundary condition and the Bernoulli equation. It can be seen from the figures that the results without the effect of gravity are very close to those with gravity effect. In fact, as discussed by Korobkin & Wu (2000), at the initial stage of impact, the effect of gravity is of second order τ^2. It has also been shown by Sun *et al.* (2015) through detailed numerical simulations that the gravity effect is small at initial stage. The largest τ here in Fig. 6c is 0.0404 and the fact that the gravity is insignificant is consistent with what has been observed previously.

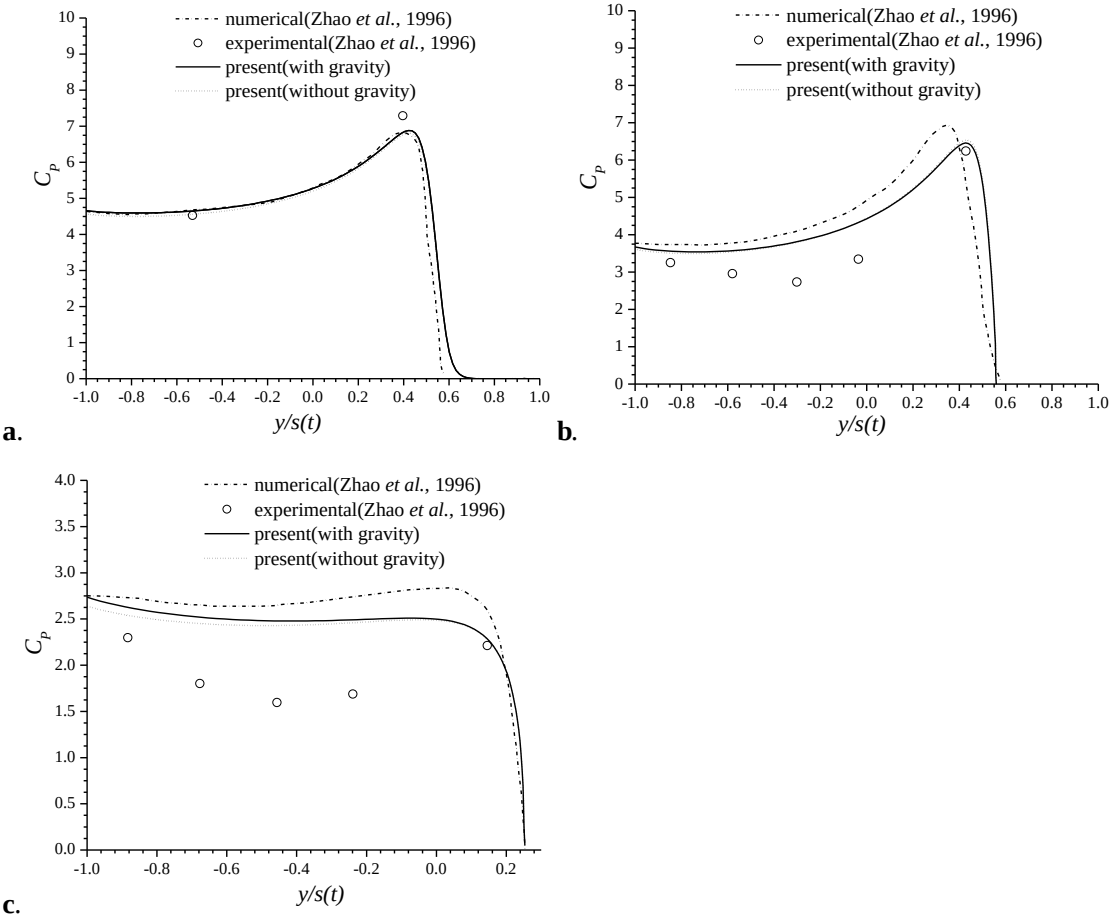

Fig. 6 Comparison of pressures (a) $\tau = 0.0087$, (b) $\tau = 0.0316$ and (c) $\tau = 0.0404$

3.2 Vertical entry of a symmetric body

We undertake more detailed study for the wedge considered in Fig. 3 with a constant vertical speed of F_n=2. Fig. 7a shows the free surface profiles at different τ. At early stage a thin jet is fully attached to the body surface. The area of the wetted surface increases with constant speed until

the flow detaches from the knuckle at around τ =0.2. Due to the momentum, the jet departed from the knuckle maintains its shape initially. When the jet root has departed from the body surface, the free surface shape begins to change significantly. We also ought to point out that as τ is no longer as small as those in Fig.6, the gravity effect becomes important too. As τ increases, the freesurface shape near the body begins to resemble that of steady cavity flow behind a wedge (Gurevich, 1965). The jet on the other hand has moved farther away from the body and becomes even thinner. The flow inside the thin jet is treated using the method in Section 2.4.

The pressure distribution is presented in Fig. 7b. The jet departs from the knuckle at around $\tau = 0.2$. The pressure distribution at this stage is virtually the same as that from the attached flow (Sun *et al.*, 2015). A large pressure gradient can be observed near the jet root, which corresponds to a large acceleration due to the sharp change of the flow direction (Sun *et al.*, 2015). As τ increases, the jet root moves up along the wedge surface and therefore the large pressure gradient also moves up. This continues until the jet root has departed from the knuckle. From then, the pressure variation along the body surface becomes much milder as can be seen from the results for τ >0.4. As τ increases further, the temporal variation of the pressure also becomes small. In fact, when the gravity effect is ignored, the solution would be expected to tend to the steady cavity solution (Gurevich, 1965).

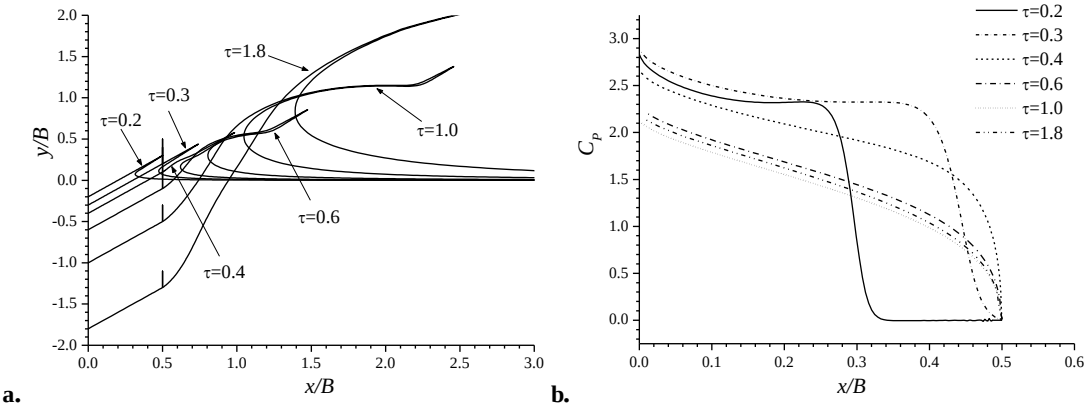

Fig.7 Vertical entry of a wedge ($\gamma = \pi/4, \theta = 0$) with F_n=2, (a) free surface profile,(b) pressure distribution on the wedge surface

When the jet moves away from the wedge, it may become extremely thin in the numerical simulation. Both sides of the jet have virtually merged to become a sheet. We may remove the jet at this stage as it has virtually no effect on the results. A line element can be used at the truncation to connect the free surfaces on the two sides. An example of jet cutting is shown in Fig. 8a. The pressures on the wedge surface with and without jet cutting are given in Fig. 8b and then are graphically identical.

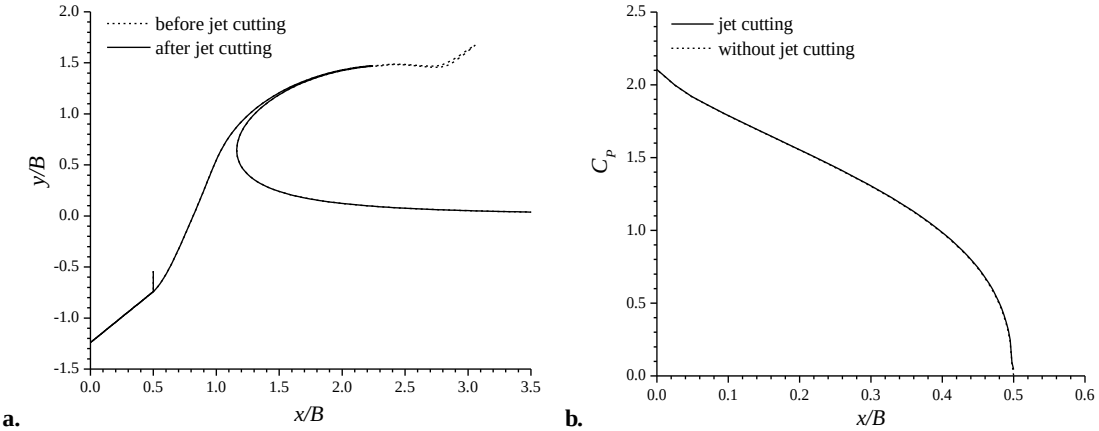

Fig. 8 Pressure comparison (same as Fig. 7) at τ =1.24, (a) free surface profile,(b) pressure distribution on the wedge surface

We notice that the effect of the gravity is unimportant when $gt \ll V$ in the dimensional sense, or $\tau \ll F_n^2$ in the non-dimensional sense. Beyond that, the gravity will become important. To investigate this, we provide results of free-surface profile and pressure on the wedge surface for F_n =1, 2 and 3 at τ =1.0 and τ =1.8, respectively, in Figs. 9 and 10. Based on the above condition, it is expected that the gravity is already important for F_n =1 at τ =1.0 and τ =1.8. In fact, Fig. 9ashows that the free surface at F_n =1 is much lower than those at F_n =2 and F_n =3. At larger τ =1.8 in Fig. 9b the larger gravity effect at F_n =1 is in fact moving the free surface towards the center. It can be expected as τ increases further and further, the open cavity will become a closed one eventually. At larger F_n, the effect of gravity will be reduced. This explains the small difference between the free surface shapes for F_n =2 and F_n =3 at a smaller τ =1.0 in Fig. 9a. Based on the condition above, at larger τ =1.8 in Fig. 9b, the difference becomes more obvious. However they are still much closer than the curve corresponding to F_n =1.0. Evidently, as τ continues to increase, the open cavity will become a closed one at any finite Froude number eventually. However, before that happens, at a sufficiently large F_n, the free surface will be closer and closer to that of the steady cavity flow (Gurevich, 1965). This pattern is also reflected in the pressure distribution in Figs. 10a and 10b.

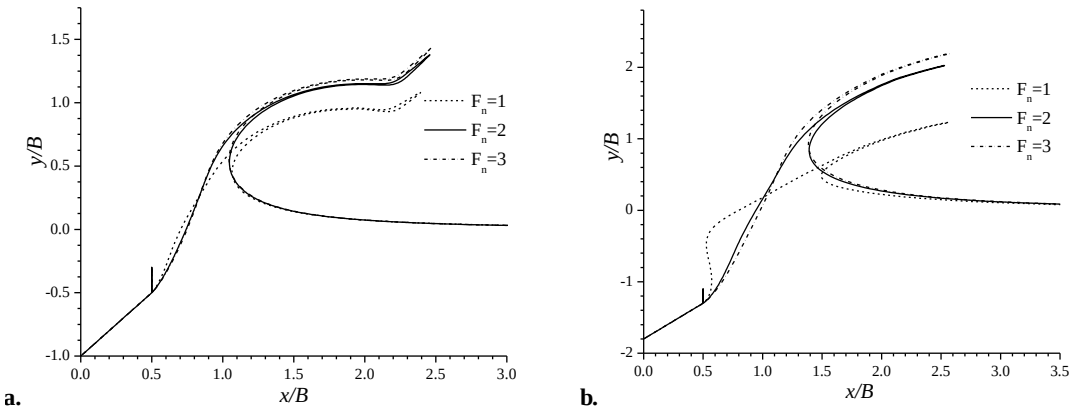

Fig. 9 The free surface profile, (a) $\tau = 1.0$, (b) $\tau = 1.8$

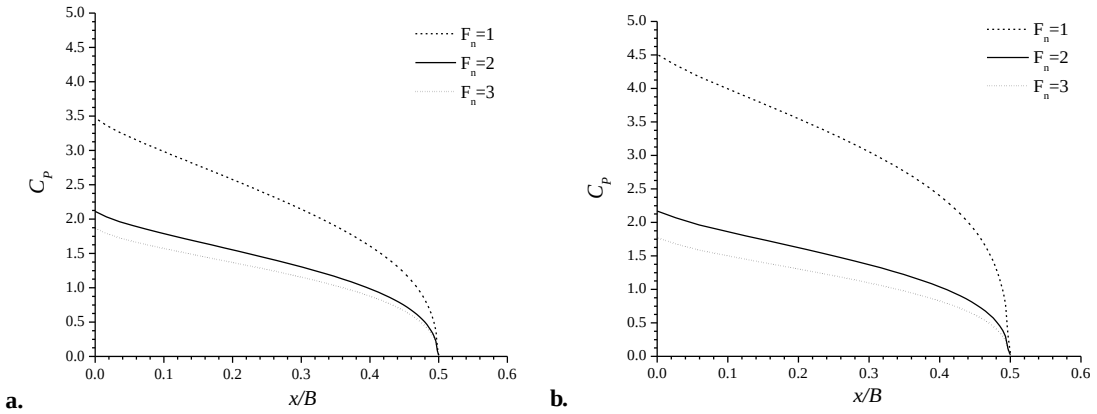

Fig. 10 The pressure distribution on wedge surface, (a) $\tau = 1.0$, (b) $\tau = 1.8$

3.3 Vertical entry of an asymmetric body

We now consider vertical entry of an asymmetric wedge with $\gamma = \pi / 4$ and different θ at F_n=2. γ_1 and γ_2 are obtained from Eq. (1), respectively. Fig. 11a shows the free surface profiles at τ =0.3. We can see that when $\theta < 10^\circ$, the jet roots on both sides of the wedge are still on the surface. The patterns of the pressure distribution resemble that of the flow attached to the body surface, i.e., a sharp pressure gradient at the jet root to change the flow direction. At $\theta = 15^\circ$, the jet root on the right side of the wedge has just left the knuckle at τ =0.3 in Fig. 11a and therefore its corresponding pressure gradient in Fig. 12a becomes less steep. At τ =0.6 in Fig. 11b, all the jet roots have left the knuckle and the sharp gradient has disappeared from all the pressure curves in Fig. 12b.

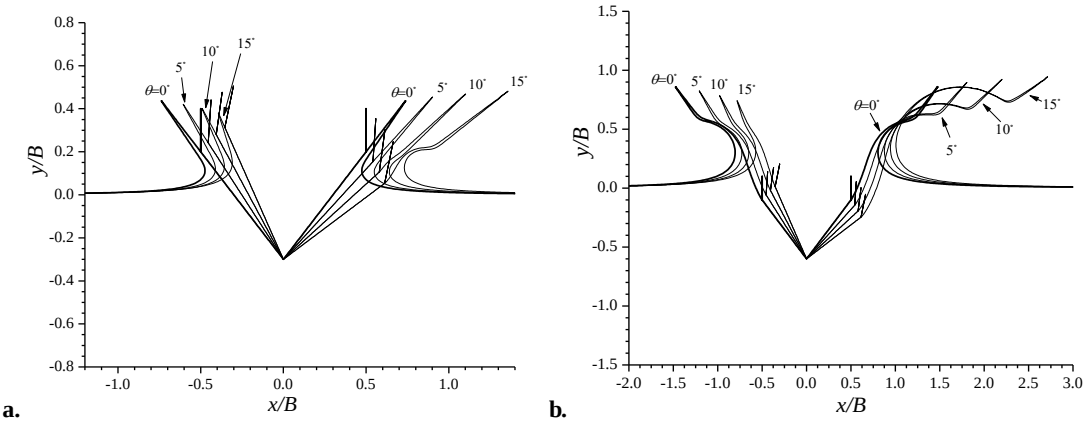

Fig. 11 The free surface profile($\gamma = \pi / 4$, F_n =2), (a) $\tau = 0.3$, (b) $\tau = 0.6$

Deadrise angle has major effect on the pressure on the wedge surface. As $\gamma_2 < \gamma_1$, the pressure on the right hand side is larger than that on the left. The difference increases as the difference between γ_2 and γ_1 increases. Because of the asymmetry of the flow, there will be velocity singularity at the tip of the wedge. The pressure near the tip changes rapidly, similar to that in the attached flow (Xu *et al.*, 2008). This could be treated through Kutta condition with vortex shedding (Xu & Wu, 2015). However it is beyond the scope of the current work.

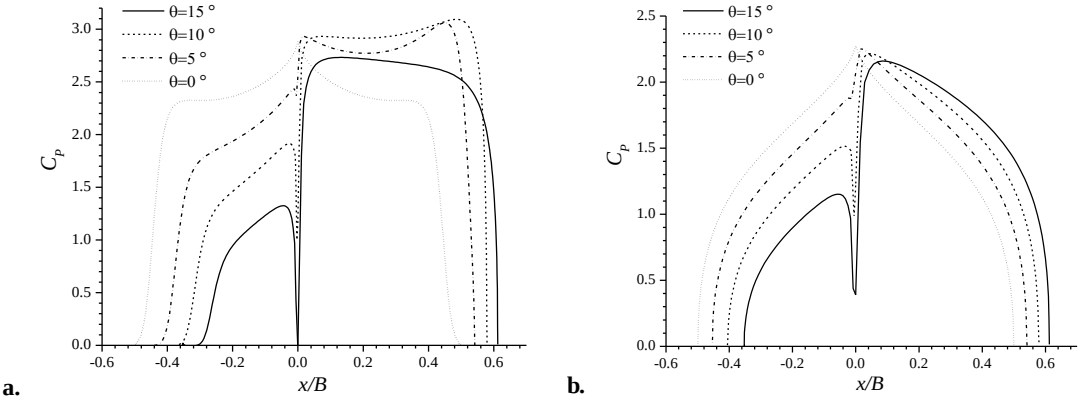

Fig. 12 The pressure distribution on wedge surface ($\gamma = \pi / 4$, F_n =2), (a) $\tau = 0.3$, (b) $\tau = 0.6$

3.4 Oblique entry

We then consider oblique entry at different $\varepsilon = U / V$. Figs. 13 give the free surface profile at τ =0.6 and τ =1.2 respectively. As body pushes the liquid along the ***x*** direction, the elevation of the free surface on the right hand side flow is higher than that on the left, and the difference increases as ε increases. This is also reflected by the pressure in Fig. 14. The pressure varies rapidly near the tip of the wedge because of the cross flow as in the cases in the previous section. The variation becomes more rapidly as ε increases.

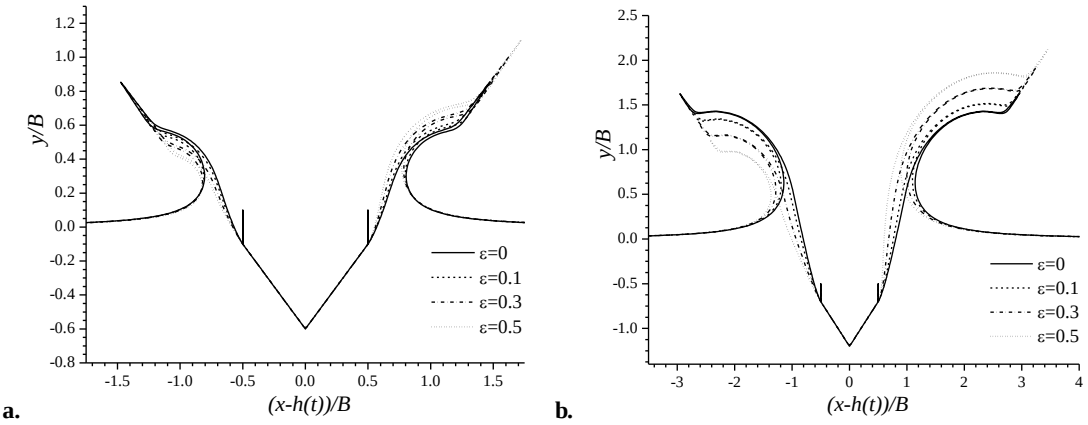

Fig. 13 The free surface profile($\gamma = \pi / 4$, $\theta = 0$, F_n =2), (a) $\tau = 0.6$, (b) $\tau = 1.2$

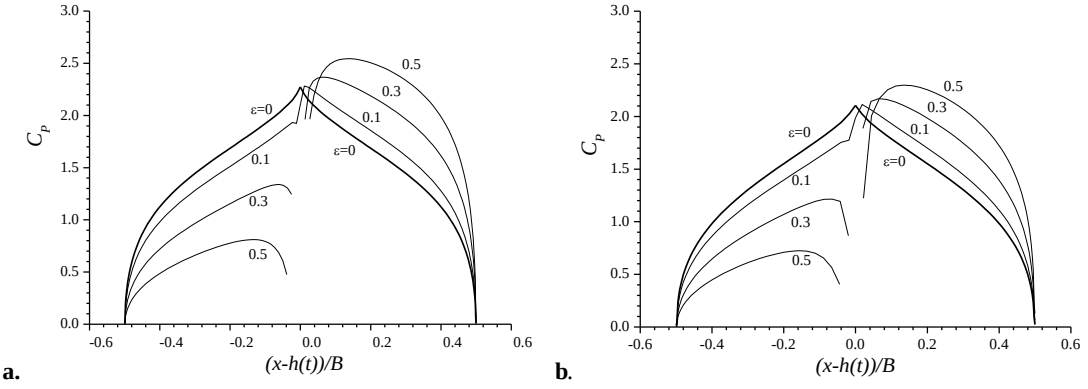

Fig. 14 The pressure distribution on wedge surface ($\gamma = \pi / 4$, $\theta = 0$, F_n =2), (a) $\tau = 0.6$, (b) $\tau = 1.2$

We notice that in the above case if we look the flow on the wedge, the angle between the direction of the incoming flow and the right hand side of the wedge is $\gamma - \text{actan}(U/V)$, and the angle with the left is $\gamma + \text{actan}(U/V)$. If we consider vertical entry of a wedge of same inner angle and $\theta = \text{actan}(U/V)$, the relative directions between the flow and the symmetry line of the wedge in both cases are the same. In Fig.15, we provide results for oblique entry of a symmetric wave with $\varepsilon = 0.2679$ and vertical entry of a symmetric wedge with $\theta = \text{actan}\,\varepsilon = 15^\circ$. From the figure, we can see that the results at smaller τ =0.3 are very different. This is because although the relative flow directions are same, the free surface effect is different. As τ increases, the two set of results become closer (it should be noted that the real comparison for the free surface should be made after turning the curve of $\theta = 15^\circ$ by 15° anti-clockwise). At τ =2.7, the pressure curves in these two cases become very close, as the effect of the free surface begins to diminish. As $\tau \to \infty$, it is expected that these to curves will become identical.

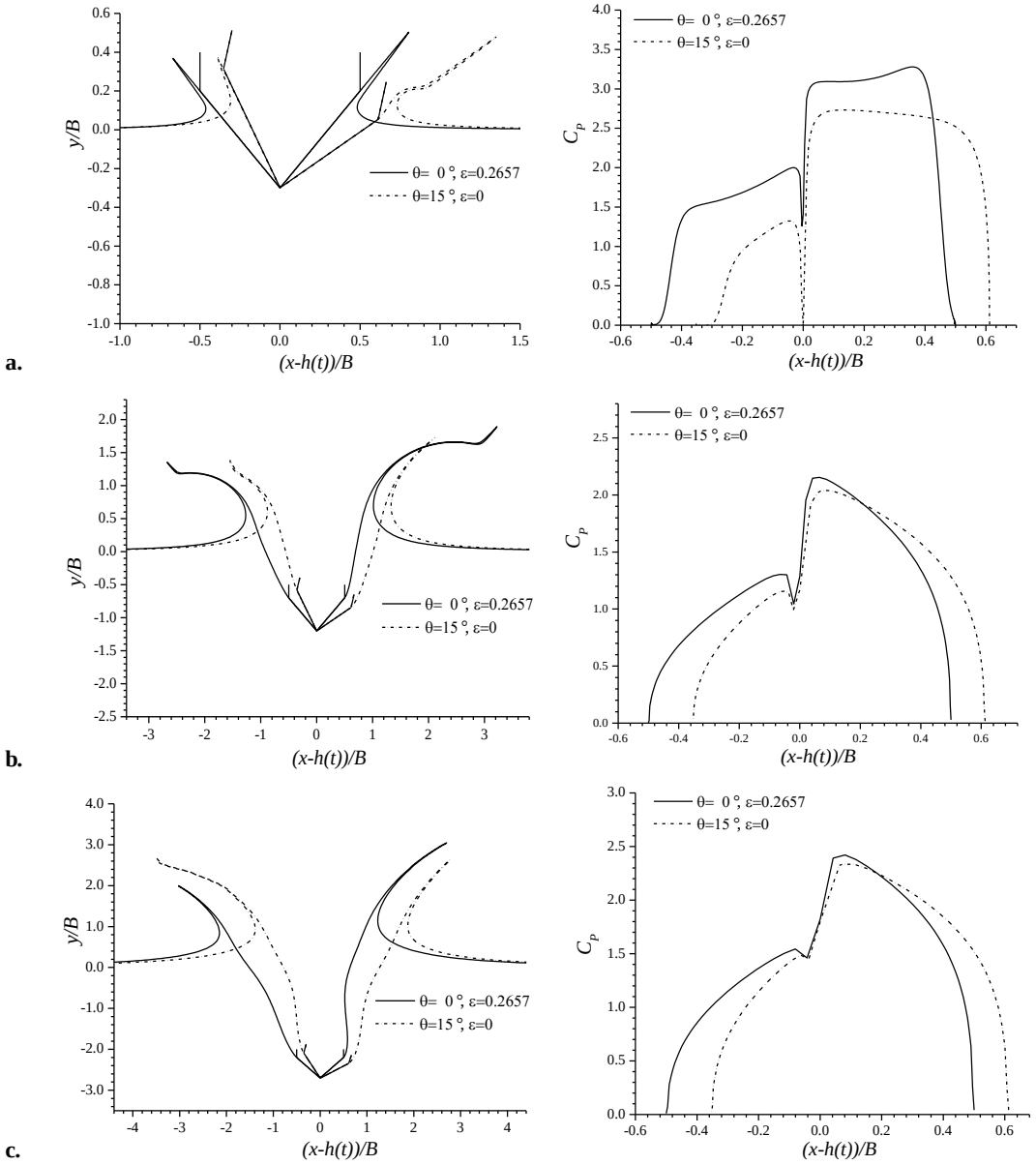

Fig. 15 Free surface profile and the pressure on the wedge surface ($\gamma = \pi / 4$, F_n =2) at: (a) τ =0.3, (b) τ =1.2, (c) τ =2.7

Following the above example, it would be interesting to consider a case of oblique entry of an asymmetric wedge, in which the wedge is symmetric about the flow direction. We choose a wedge of $\gamma = \pi / 4$ and $\theta = -15^\circ$, with $\varepsilon = \tan 15^\circ = 0.2679$. Fig. 16a gives the free surface profiles. The flow is asymmetric at smaller τ =0.3 due to different deadrise angles on the two sides of the wedge relative to the free surface. This is also reflected by the pressure in Fig. 16b. As τ increases, the asymmetry has decreased significantly (the symmetry in Fig. 16a should be viewed about the flow direction). In fact at τ =2.7 the rapid variation of pressure at the tip of the wedge begins to disappear, as the free surface begins to disappear. It ought to point out that the discussions about Figs. 15 and 16 are for a relatively large F_n, with $\tau \ll F_n^2$. This means that the gravity effect is yet to show its importance. Without the gravity, the result will tend to the steady cavity flow. With the gravity, a

closed cavity may be formed. However, the focus of our work is on impact, which is usually for small τ. The flow at very large τ is beyond the scope of the current paper.

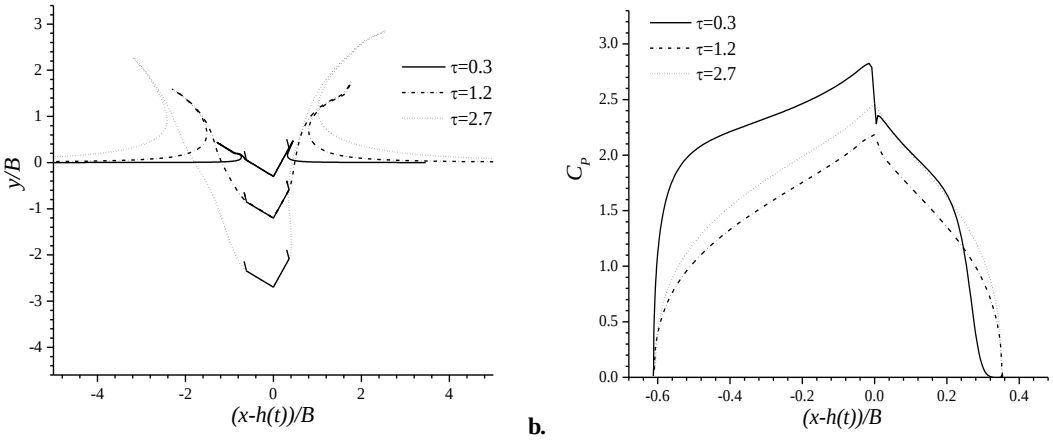

Fig. 16 Oblique entry of a wedge symmetric about the main flow direction ($\gamma = \pi / 4$, $\theta = -15^\circ$, F_n=2) at $\varepsilon = 0.2679$, (a) the free surface profile and, (b) the hydrodynamic pressure distribution on the wedge surface

4. Conclusions

Based on velocity potential theory with fully nonlinear boundary conditions, the problem of a finite wedge entering water with flow separation is solved by using the boundary element method. Before flow separation, the jet attached on the free surface is treated using the exiting shallow water equation. After flow separation, a new methodology is introduced for the free jet, which can provide the velocity of the jet directly without the need of finding it through the boundary element method. Through the obtained results, we can draw the following conclusions.

(1) The gravity effect is unimportant when $\tau \ll F_n^2$. Thus as the entry speed increases, the gravity effect can be ignored over a long period of time, during which the flow gradually tends to the steady cavity flow behind a wedge.

(2) The pressure distribution after the flow separation is very different from that before the separation. In particular, when the jet root has passed the knuckle, a large gradient of pressure no longer exists on the body surface, as it is on longer required to turn the flow direction sharply.

(3) The pressure varies rapidly near the tip of the wedge when the flow is asymmetric. However when the relative direction of the main flow is along the symmetry line, the flow across the tip, which may exist initially due to the difference in the deadrise angles on both sides, will decrease. As time progresses the discontinuity of the pressure at the tip gradually disappears, on the basis $\tau \ll F_n^2$.

Acknowledgements

This work is supported by Lloyd's Register Foundation through the joint centre involving University College London, Shanghai Jiaotong University and Harbin Engineering University, to

which the authors are most grateful. Lloyd's Register Foundation helps to protect life and property by supporting engineering-related education, public engagement and the application of research.

This work is also supported by the National Natural Science Foundation of China (Grants No. 11472088 and 51479044).

References

Dobrovol'skaya, Z. N. 1969 Some problems of similarity flow of fluid with a free surface. J. Fluid Mech. 36, 805–829.

Gu, H. B., Qian, L., Causon, D. M., Mingham, C. G., & Lin, P. 2014. Numerical simulation of water impact of solid bodies with vertical and oblique entries. Ocean Engineering, 75, 128-137.

Greenhow, M., & Lin, W. M. 1983. Nonlinear Free Surface Effects: Experiments and Theory. Report No. 83–19 Cambridge, Massachusetts: Dept. Ocean Eng., Mass. Inst. Technol.

Gurevich, M. I. 1965. Theory of Jets in Ideal Fluids. Academic Press, New York

Judge, C., Troesch, A., & Perlin, M. 2004. Initial water impact of a wedge at vertical and oblique angles. Journal of Engineering Mathematics, 48(3-4), 279-303.

Korobkin, A.A., Wu, G.X., 2000. Impact on a floating circular cylinder. Proceedings of the Royal Society of London A456, 2489–2514.

Lu C.H., He Y.S., Wu G.X., 2000. Coupled analysis of nonlinear interaction between fluid and structure during impact. Journal of Fluids and Structures 14, 127-146.

Oger, G., Doring, M., Alessandrini, B., & Ferrant, P. 2006. Two-dimensional SPH simulations of wedge water entries. Journal of computational physics, 213(2), 803-822.

Semenov, Y. A., & Iafrati, A. 2006. On the nonlinear water entry problem of asymmetric wedges. Journal of Fluid Mechanics, 547, 231-256.

Sun, H., & Faltinsen, O. M. 2007. The influence of gravity on the performance of planing vessels in calm water. Journal of Engineering Mathematics, 58(1-4), 91-107.

Sun, H. 2007. A boundary element method applied to strongly nonlinear wave-body interaction problems. PhD thesis, Norwegian University of Science and Technology.

Sun, S. Y., Sun, S. L., & Wu, G. X. 2015. Oblique water entry of a wedge into waves with gravity effect. Journal of Fluids and Structures, 52, 49-64.

Tassin, A., Korobkin, A. A., & Cooker, M. J. 2014. On analytical models of vertical water entry of a symmetric body with separation and cavity initiation. Applied Ocean Research, 48, 33-41.

Wu, G. X., 1998. Hydrodynamic force on a rigid body during impact with liquid. Journal of Fluids and Structures 12, 549–559.

Wu, G. X., & Taylor, R. E. 2003. The coupled finite element and boundary element analysis of nonlinear interactions between waves and bodies. Ocean Engineering, 30(3), 387-400.

Wu, G. X., Sun H., &He Y.S., 2004. Numerical simulation and experimental study of water entry of a wedge in free fall motion. Journal of Fluids and Structures 19, 277-289.

Wu, G. X., 2007. Two-dimensional liquid column and liquid droplet impact on a solid wedge. The

Quarterly Journal of Mechanics and Applied Mathematics, 60(4), 497-511.

Xu, G. D., Duan, W. Y., & Wu, G. X. 2008. Numerical simulation of oblique water entry of an asymmetrical wedge. Ocean Engineering, 35(16), 1597-1603.

Xu, G. D., &Wu, G. X. 2015. Oblique water entry of a wedge with vortex shedding, Procceedings of the International Workshop on Water Waves and Floating Bodies, Bristol.

Zhao,R. & Faltinsen, O. M. 1993. Water entry of two-dimensional bodies. J. Fluid Mech. 246, 593–612.

Zhao, R., Faltinsen, O., & Aarsnes, J. 1996. Water entry of arbitrary two-dimensional sections with and without flow separation. In Proceedings of the 21st symposium on naval hydrodynamics (pp. 408-23). Trondheim, Norway, National Academy Press, Washington, DC, USA.